Biosensors and Bioelectronics 74 (2015) 967–973

Contents lists available at ScienceDirect

Biosensors and Bioelectronics

journal homepage: www.elsevier.com/locate/bios

Constructing heterostructure on highly roughened caterpillar-like gold nanotubes with cuprous oxide grains for ultrasensitive and stable nonenzymatic glucose sensor

Anran Chen [a], Yu Ding [a], Zhimao Yang [a,b], Shengchun Yang [a,b,*]

[a] MOE Key Laboratory for Non-Equilibrium Synthesis and Modulation of Condensed Matter, State Key Laboratory for Mechanical Behavior of Materials, Xi'an Jiaotong University, Xi'an 710049, People's Republic of China

[b] Collaborative Innovation Center of Suzhou Nano Science and Technology, Suzhou Academy of Xi'an Jiaotong University, 215000 Suzhou, People's Republic of China

ARTICLE INFO

Article history:
Received 28 March 2015
Received in revised form
27 July 2015
Accepted 30 July 2015
Available online 31 July 2015

Keywords:
Heterostructure
Cu_2O grains
Caterpillar-like Au nanotubes
Glucose biosensor

ABSTRACT

In this study, a metal–metal oxide heterostructure was designed and constructed by growing cuprous oxide (Cu_2O) grains on highly surface roughened caterpillar-like Au nanotubes (CLGNs) for ultrasensitive, selective and stable nonenzymatic glucose biosensors. The Cu_2O grains are tightly anchored to the surface of CLGNs by the spines, resulting in a large increase in the contact area between Cu_2O grains and the CLGNs, which facilitates the electron transport between metal and metal oxide and improves the sensitivity and stability of the sensors. The electron transfer coefficient (α) and electron transfer rate constant (k_s) for redox reaction of Cu_2O–CLGNs/GCE are found to be 0.50114 and $3.24 \pm 0.1\ s^{-1}$, respectively. The biosensor shows a linear response to glucose over a concentration range of 0.1–5 mM and a high sensitivity of 1215.7 $\mu A\ mM^{-1}\ cm^{-2}$ with a detection limit of 1.83 μM. Furthermore, the Cu_2O–CLGNs biosensor exhibited strong anti-interference capability against uric acid (UA), ascorbic acid (AA), potassium chloride (KCl) and sodium ascorbate (SA), as well as a high stability and repeatability. Our current research indicates that the Cu_2O–CLGNs hybrid electrode is a promising choice for constructing nonenzyme based electrochemical biosensors.

1. Introduction

Effective and reliable detection of glucose is of great significance in food analysis, brewing, biotechnology and medical diagnosis (Chen and Chatterjee, 2013). In the past few decades, the glucose oxidase was recognized as an efficient and popular choice for enzymatic glucose biosensor because of its high selectivity, good sensitivity and faster response (Minteer et al., 2012). However, several disadvantages of the enzyme-modified electrodes have been found in long-term clinical practice, such as instability, unsatisfactory reproducibility, high cost and insufficient long-term stability of the enzymes, and complicated immobilization procedure (Ahmad et al., 2013; Xu et al., 2013; Zhang et al., 2014c). To overcome these drawbacks, the electrocatalytic oxidation of glucose without the use of enzymes has attracted increasing attentions in recent years. Therefore, more and more new electrode materials as possible alternatives to glucose oxidase have been developed, and the kinetics and mechanism of glucose electro-oxidation on the as-designed electrode have been intensively investigated, showing that three major questions need to be well resolved (Lang et al., 2013; Minteer et al., 2012; Yang and Luo, 2014; Yang et al., 2010): (1) mass diffusion of analyte at the interface between electrolyte and electrode and in inner electrode, which greatly affected the kinetics of the glucose electro-oxidation; (2) the catalytic performance of the electrode materials, which decided the activity, selectivity and stability of the electrode; (3) the charge-transport and electron-transfer at the electrolyte/electrode interface, and the electron conduction in electrode and current collector, which largely determined their sensitivity and detectability.

The noble metal based nanostructures have elicited much interest for glucose non-enzymatic electrochemical determinations, due to their particular catalytic activity and well stability (Chen and Chatterjee, 2013). Therefore some recent efforts have been made for non-enzymatic sensors by immobilizing a variety of noble metal nanoparticles onto electrodes, such as platinum, gold, silver and their alloy (Ahmadalinezhad et al., 2013; Cao et al., 2013; Hsu and Wang, 2014; Li et al., 2014a, 2014b; Liu et al., 2013b; Niu et al., 2012; Wang et al., 2008; Xu et al., 2013, 2010; Yang et al.,

* Correspondence to: School of Science, Xi'an Jiaotong University, 28#, Xi'anning Xilu, Xi'an, Shannxi 710049, People's Republic of China.
E-mail addresses: zmyang@mail.xjtu.edu.cn (Z. Yang), ysch1209@mail.xjtu.edu.cn (S. Yang).

http://dx.doi.org/10.1016/j.bios.2015.07.074
0956-5663/

2014b; Yu et al., 2010). However, a relatively low selectively, resulting from the electrochemical sensitivity of noble metals toward the small organic molecules, was not favorable to their practical applications. Nanostructured metal oxides, due to their low cost, highly specific surface area, good electrochemical activity, and the possibility of promoting electron transfer reactions at a lower overpotential (Cherevko and Chung, 2010; Ci et al., 2014; Liu et al., 2013a), have been proved to be promising materials for fabricating nonenzymatic glucose sensors. However, one of the inevitable limitations for the metal oxides is their poor electronic conductivity, which significantly affected the sensitivity, reliability and even selectivity of the biosensors made of these materials (Ding et al., 2010a; Duan et al., 2008).

In recently years, combining the nanostructured metal oxides with a substrate material with high conductivity, such as metal (Lang et al., 2013; Xiao et al., 2013), carbon nanotube (Hwa and Subramani, 2014; Yang et al., 2010), graphene (Wang et al., 2014; Zhou et al., 2014) and conductive fiber (Meng et al., 2013), has been widely investigated. Studies have shown that these nanocomposites exhibit a synergistic electrocatalytic activity, especially for the noble metal nanostructures being paired with metal oxides. At the same time, the electron transfer in the electrode can be greatly promoted due to good electrical conductivity of noble metals, thus inducing a much enhanced performance toward glucose detection (Xiao et al., 2013; Lang et al., 2013).

Among various metal oxides, Cu_2O have been extensively investigated as electrode materials for constructing nonenzyme biosensors because they can function as efficient catalysts for the electrocatalytic oxidation of glucose resulting from the redox couple of $Cu^{3+}/Cu^{2+}/Cu^{+}$ in the alkaline medium (Huo et al., 2014; Luo and Baldwin, 1995; Sun et al., 2013; Torto et al., 1999; Zhou et al., 2014). Furthermore, Cu_2O crystals with well-defined sizes and shapes have been widely reported (Feng et al., 2014; Sun et al., 2010; Zhang et al., 2014a), and they have many special advantages, for example, easily controlled structures, cost saving, morphological multiformity, as well as large-scale production, which can be easily accessed and employed in the biosensor applications (Chang and Zeng, 2004; Hong et al., 2011; Kuo and Huang, 2010). Therefore, combining the advantages of both Cu_2O crystals and noble metals should be a viable option for glucose biosensor applications. However, to the best of our knowledge, there are only few studies that combine the Cu_2O nanocrystals and metal nanostructures to assess their performance in glucose electrochemical detection. Recent studies have shown that the catalytic behavior of Cu/Cu_2O hollow microspheres and reticular-vein-like $Cu@Cu_2O$/rGO nanocomposites toward the electrochemical oxidation of glucose was obviously superior to the pure Cu_2O (Huo et al., 2014; Wang et al., 2012). However, their long time stability and reproducibility are doubtful, because of the easy oxidation of metallic Cu in nanoscale. Hua et al. (2011) reported that the Cu_2O–Au nanocomposites demonstrated a much enhanced performance in enzyme-free glucose sensing compared with the pure Cu_2O nanoparticles. However, due to the gold nanoparticles loaded on the Cu_2O crystals being isolated, the enhancement in their sensing performance was largely ascribed to the polarization effect provided by Au nanoparticles, rather than the electron conduction in electrode, therefore, their sensitivity and detectability was largely restricted. In addition, the erosion of metal oxide, owing to lack of protection and easy shedding from the conductor during the measurement, also greatly affected the stability of the biosensors.

In this paper, we have constructed a novel glucose biosensor based on Cu_2O–CLGNs nanocomposite modified electrode. Cu_2O–CLGNs nanocomposite was synthesized through a seeding growth approach in which the Cu_2O nanocrystals were intimately anchored to the surface of CLGNs through ultrafine spines, thus largely enhanced the stability of Cu_2O nanocrystals on the electrode so as to improve the stability of the biosensors. In addition, due to the nature of the hollow interior and ultra roughened surface, the electrochemical active area (ECSA) of the electrode and the contact area between conductive substrate, i.e. CLGNs and metal oxide, was greatly increased, which was much conducive both to the mass transfer and electron transfer of the electrode and thus enhancing the sensitivity of the sensors.

2. Experimental

2.1. Chemicals

Poly(vinylpyrrolidone) (PVP, Average MW of 30000, Sinopharm Chemical Reagent Co. Ltd.) was used as capping agent. $AgNO_3$ ($\geq$ 99.8%, Shanghai Qiangshun Chemical Reagent Co. Ltd.) and 1,2-propylene glycol (1,2-PG, Sinopharm Chemical Reagent Co. Ltd.) were used as the source material and the reductant. 3,4-dihydroxyphenylalanine (DOPA, 98%, Aladdin Industrial Corporation) was used as reducing and the structure-directing agent. Sodium dodecyl sulfate (SDS, $\geq$ 99.8%, Sinopharm Chemical Reagent Co. Ltd.), $Cu(NO_3)_2 \cdot 3H_2O$ and NaOH were obtained from Aladdin Industrial Corporation. Hydrazine hydrate ($N_2H_4 \cdot 2H_2O$, $\geq$ 99.8%) was purchased from Shanghai Qiangshun Chemical Reagent Co. Ltd. Chlorauric acid trihydrate ($HAuCl_4 \cdot 3H_2O$, analytical grade) was obtained from Sino-Platinum Co. Ltd. All chemicals used in experiment were used as-received without further purification. Deionized water (18.25 MΩ cm) was used in all of the preparations.

2.2. Synthesis of caterpillar-like Au nanotubes

The caterpillar-like Au nanotubes were synthesized as our previous report (Yang et al., 2014a). Firstly, Ag NWs were synthesized by reducing silver nitrate in the presence of PVP in EG (Bi et al., 2010). In brief, 1,2-propylene glycol (1,2-PG, 10 mL) contained with PVP (150 mM, as calculated in terms of the repeating unit) was placed in a 25 mL vial, capped and heated at 160 °C under vigorous stirring for 1 h. Then 1 mL of NaCl solution (1 mM in 1,2-PG) was quickly added. After 5 min, 4 mL of $AgNO_3$ (150 mM in 1,2-PG) was added dropwise to the stirring solution. The vial was then capped and heated at 160 °C for 40 min. The product was separated by centrifugating at 4000 rpm for 3 min, and the precipitate was centrifuged some times in deionized water and anhydrous ethanol, respectively. The Ag nanowire was dispersed into deionized water. In a typical synthesis of caterpillar-like Au nanotube, 0.2 mL of a colloidal solution of Ag NWs was mixed with 13.5 mL of water in a 25 mL glass vial under vigorous stirring at a speed of 450 rpm and the room temperature. Then, 1.25 mL of chlorauric acid (40 mM) was quickly added. After 30 s, 5 mL of an aqueous solution of 3,4-dihydroxyphenylalanine (DOPA, 10 mM) was added immediately. After 10 min, the caterpillar-like Ag nanotubes were centrifuged, washed with deionized water several times. The final product was dispersed into deionized water.

2.3. Synthesis of Cu_2O–CLGNs hybrid nanomaterials

The Cu_2O–CLGNs hybrid nanomaterials were prepared by a modified seeding growth process in aqueous solution. In a typical procedure, 3 mg of $Cu(NO_3)_2 \cdot 3H_2O$ and 0.0721 g of SDS were dissolved in 20 mL of H_2O under vigorous stirring for 3 min, then 1 mL of CLGNs solution was added dropwise and stirring for 2 min, followed by slow addition of 0.02 g of NaOH dissolved in 5 mL of deionized water. After stirring at 25 °C for 20 min, 5 mL of deionized water containing 10 μL of hydrazine hydrate ($N_2H_4 \cdot 2H_2O$)

was added dropwise into the mixture under magnetic stirring (350 rpm). After 40 min of reaction, the product was collected by centrifugating at 6000 rpm for 2 min, and washed with deionized water and ethanol three times, respectively.

2.4. Electrochemical measurements

A nonenzyme amperometric electrochemical sensor was prepared by coating Nafion/Cu_2O–CLGNs sample onto a glassy carbon electrode (GCE) at room temperature. The modified electrode was prepared as follows: 20 μL of the suspension with dispersed Cu_2O–CLGNs or CLGNs was dropped on the pre-treated glassy carbon electrode and dried at room temperature. Then, 20 μL Nafion solution (0.05%, Sigma-Aldrich) was dropped on the surface of electrodes and dried at room temperature. Before modification, the bare GCE (5.0 mm in diameter) was polished to a mirror-like surface with 0.5 μm and 50 nm alumina powder, and then washed ultrasonically in deionized water, ethanol and deionized water for a few minutes. The modified electrode was used as the working electrode, a platinum foil as the counter electrode and Ag/AgCl as the reference electrode. The blank GCE electrode was prepared by casting 20 μL Nifion solution (0.05%) on the surface of GCE electrode and left it to dry at room temperature.

2.5. Characterization

The morphology of the products was investigated by field emission scanning electron microscope (FESEM, JEOL, JSM-7000F) at an acceleration voltage of 20 kV. Powder X-ray diffraction (XRD) pattern was recorded on a Bruker-AXS D8 Advance diffractometer operated at 40 kV voltage and 40 mA current using Cu Kα radiation ($\lambda = 1.5406$ Å) in the range of 15–90°. The transmission electron microscope (TEM) analysis was performed on a JEOL JEM-2100 transmission electron microscope operated at an accelerating voltage of 200 kV. Samples for TEM analysis were prepared by ultrasonic dispersion for 10 s with water. Then, the products were dropped onto a carbon-coated copper grid and dried in air before the TEM analysis.

3. Results and discussion

3.1. Structure and morphology of silver NWs, CLGNs and hybrid Cu_2O–CLGNs

The surface morphologies of silver NWs, CLGNs and hybrid Cu_2O–CLGNs were explored using FESEM and TEM, as presented in Fig. 1. Fig. 1A shows the SEM images of the as-synthesized Ag nanowires, which indicates a long and smooth morphology with a uniform diameter throughout the length of the nanowire. The average diameter is estimated to be about 40 nm. Herein, DOPA, as reported elsewhere (Xu et al., 2010), was used as both reducer and inducing agent for the preparation of CLGNs in aqueous solution at room temperature, as well as silver nanowires were used as the sacrificial template. As shown in Fig. 1B, the SEM image shows that the nanotubes present a prickly surface with a diameter of about 250 nm, quite similar with that of a caterpillar, as we have described in our previous work (Yang et al., 2014a). Hybrid Cu_2O–CLGNs was prepared through the reduction of $Cu(OH)_4^{2-}$ by $N_2H_4 \cdot 2H_2O$ using spiky Au NTs as seeds. SEM and TEM images of the hybrid Cu_2O–CLGNs are shown in Fig. 1C and E, indicating the fusiform-like Cu_2O grains with diameter ranging from 100 to 200 nm being intimately immobilized onto the surface of CLGNs. The corresponding EDS analysis demonstrated the presence of copper, oxygen, gold and silicon, indicating that the Cu_2O grains were integrated with CLGNs (Fig. S1). The peak of silicon derived from the substrate surface of the sample.

Fig. 1D shows the XRD patterns of the as-prepared Cu_2O powder, Ag NWs, CLGNs and hybrid Cu_2O–CLGNs nanocomposite, respectively. For the Ag NWs and CLGNs samples, the XRD pattern

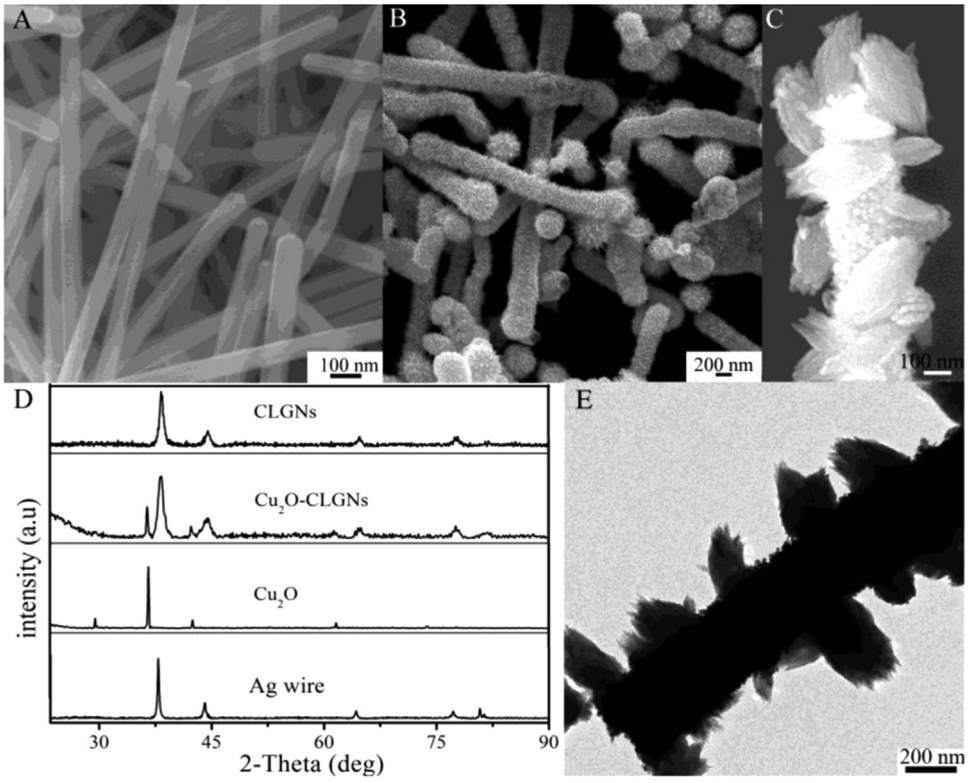

Fig. 1. FESEM images of Ag wire (A), caterpillar-like Au nanotubes (B), CLGNs nanotubes (C), and XRD images of the as-prepared material (D). (E), TEM image of Cu_2O–CLGNs.

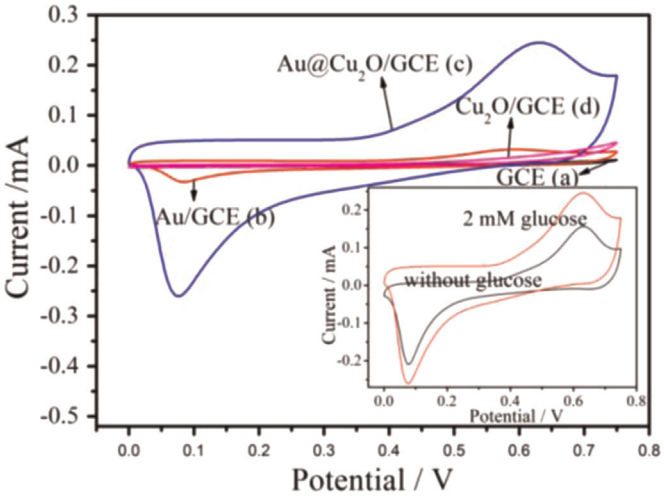

Fig. 2. Typical cyclic voltammograms of GCE (a), Au/GCE (b), Cu_2O–CLGNs/GCE (c), Cu_2O/GCE (d) electrodes in 100 mM KOH solution at scan rate of 50 mV s^{-1}. The inset shows the CVs of the Cu_2O–CLGNs/GCE electrode with and without glucose, respectively.

indicates a typical face-centered cubic (fcc) structure. As for the sample of hybrid Cu_2O–CLGNs nanocomposite, characteristic peaks of Cu_2O, locating at 29.6°, 36.5°, 42.4°, 61.5° and 73.7°, can be well identified, which is in good agreement with that of the pure Cu_2O sample, corresponding to the (110), (111), (200), (220) and (311) crystal planes of cubic Cu_2O phase (JCDS 78-2076), respectively. While the peaks located at 38.2°, 44.3°, 64.6° and 81.7° can be assigned to the (111), (200), (220) and (311) planes of the metallic gold (JCDS 04-0784). The analysis results from the XRD patterns indicate the formation of the hybrid Cu_2O–CLGNs nanocomposites.

3.2. Electrochemical behavior of the Cu_2O–CLGNs electrode

Fig. 2 shows the cyclic voltammograms (CVs) of the bare GCE, Au/GCE, Cu_2O–CLGNs/GCE and Cu_2O/GCE in 100 mM KOH solution in the presence of 2 mM glucose at a scan rate of 50 mV s^{-1}. The results indicate that the Cu_2O–CLGNs/GCE electrode presents the most significant enhancement in anodic peak current among the as-used electrodes, indicating a quite sensitive nature of the Cu_2O–CLGNs/GCE electrode toward glucose oxidation. The inset in Fig. 2 shows the CVs of the Cu_2O–CLGNs/GCE electrode with and without glucose, respectively. Both of them displayed a pair of broad reduction peaks with a peak potential of 0.63 V vs. Ag/AgCl, approximately, which corresponded to the Cu^{2+}/Cu^{3+} redox couple according to the previous report (Sun et al., 2013; Wu et al., 2010; Zhuang et al., 2008), where the released electrons formed oxidation peak currents, and then the glucose was oxidized to gluconic acid with the assistance of Cu (II) and Cu (III), which was simultaneously reduced to Cu (I) (Zhou et al., 2014). Herein, the Cu (III) species were proposed to be an electron-transfer mediator (Wang et al., 2012). Upon addition of glucose (2.0 mM), the voltammetric characteristics of the Cu_2O–CLGNs/GCE electrode changed significantly, indicating a good synergistic effect between

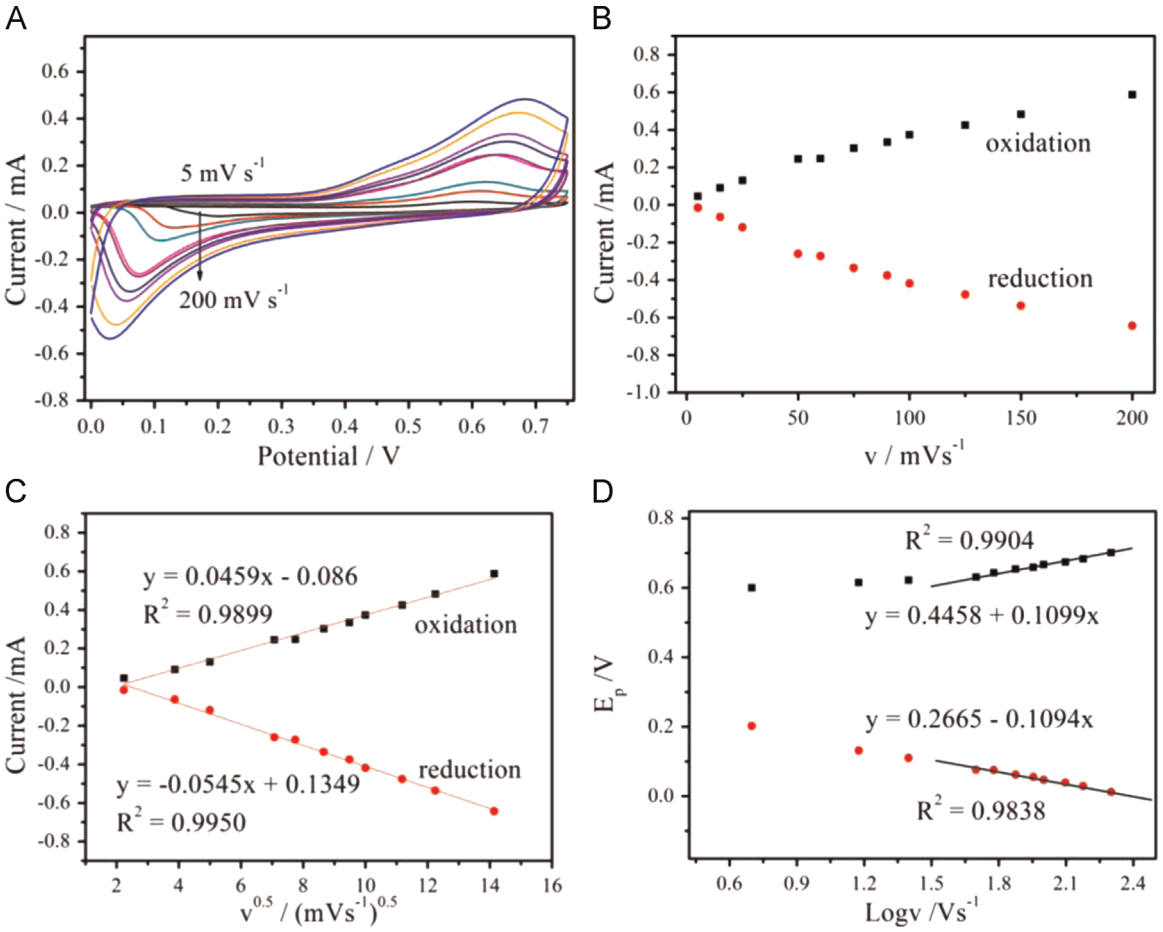

Fig. 3. (A) Typical cyclic voltammograms of Cu_2O–CLGNs/GCE in 100 mM KOH solution (containing 2 mM glucose) at different potential sweep rates of 5–200 mV s^{-1}. (B) The dependency of anodic and cathodic peak currents to the potential sweep rate. (C) Proportionality of anodic and cathodic peak currents to the square root of potential sweep rate. (D) The dependency of peak potential vs. logarithm of scan rates.

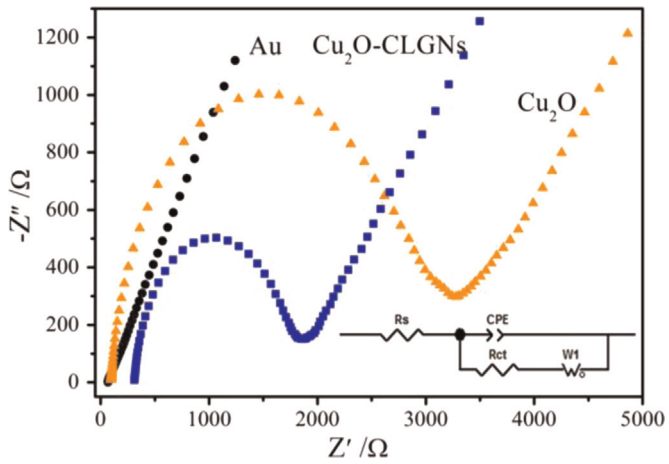

Fig. 4. Nyquist diagrams of the Au/GCE, Cu_2O–CLGNs/GCE and Cu_2O/GCE electrodes in the presence of 5 mM $K_3[Fe(CN)_6]$ with 0.1 M KCl as the supporting electrolyte.

the Cu_2O nanograins and CLGNs substrate after the hybridization. The broad and enhanced oxidation peak at around 0.6 V for Cu_2O–CLGNs/GCE electrode can be attributed to the large surface area and enhanced mass and electron transfer (Zhuang et al., 2008).

The recording of cyclic voltammograms at different potential sweep rates can be used to investigate the kinetics of glucose oxidation (Hsu and Wang, 2014). Fig. 3A shows the cyclic voltammograms of the Cu_2O–CLGNs/GCE electrode at different potential sweep rates in range of 5–200 mV s^{-1} in 100 mM KOH solution containing 2 mM glucose. It gave well symmetric anodic and cathodic peaks. When the scan rate increases, the anodic peaks slightly moved to positive direction and cathodic peaks to negative potential due to the presence of ohmic drop (Guo et al., 2014). The Fig. 3B presents the proportional of the cathodic and anodic peak currents vs. scan rate. There is a linear relationship between the peak currents and scan rates at sweep rate below 50 mV s^{-1} as expected for a surface confined redox process (Elahi et al., 2014). At the same time, the redox peak current also increases linearly and the linear regression equations can be expressed as: $I_{pa}=0.02388+0.0044x$, $R^2=0.99892$; $I_{pc}=0.01554-0.00549x$, $R^2=0.99898$, respectively. According to the equation

$$I_p = nFQv/4RT \tag{1}$$

where R is 8.314 J mol^{-1} K^{-1}, T is surrounding temperature (298.15 K), v is the scan rate, Q is the quantity of charge (C), F is Faraday constant. Integration of the area under the reduction peaks gave constant charge (Q) values independent of scan rate below 50 mV s^{-1}. These characteristics reveal that the redox reaction of Cu_2O–CLGNs/GCE electrode is a quasi-reversible surface controlled electrochemical process (Li et al., 2013). At high potential sweep rates, the peak currents are proportional to the square root of scan rate in the range of 60–200 mV s^{-1} (Fig. 3C), indicating that the redox reaction is a surface-controlled electrochemical process (Ding et al., 2011, 2010b) which is ideal for the quantitative analysis in practical applications.

Fig. 3D shows the relationship between the values of peak separation vs. Logarithm of the scan rate. The peak-to-peak separation is about 0.398 V at scan rates below 50 mV s^{-1}, suggesting charge transfer kinetics over this range of sweep rates. At higher sweep rates, peak separation increased, indicating that the limitation is due to the charge transfer kinetics. And according to the Laviron analysis, charge transfer coefficient (α) and electron transfer rate constant (k_s) can be obtained by measuring the variation of peak potential with scan rate by using Eqs. (2), (3) and (4), respectively (Huang et al., 2005).

$$E_{pa} = E^{0\backprime} + \frac{2.3RT}{(1-\alpha)nF}\log v \tag{2}$$

$$E_{pc} = E^{0\backprime} - \frac{2.3RT}{\alpha nF}\log v \tag{3}$$

$$\log k_s = \alpha\log(1-\alpha) + (1-\alpha)\log\alpha - \log\frac{RT}{nFv} - \frac{\alpha(1-\alpha)nF\Delta E_p}{2.3RT} \tag{4}$$

where R is 8.314 J mol^{-1} K^{-1}, T is surrounding temperature (298.15 K) and ΔE is the peak separation of the Cu_2O–CLGNs/GCE redox couple and n is the number of electrons transferred, here n is calculated to be 1.0778. The transfer coefficient (α) is estimated to be 0.50114. The electron transfer rate constant (k_s) of Cu_2O–CLGNs/GCE is calculated as 3.24 ± 0.1 s^{-1}, indicating fast electron transfer kinetics. The surface average concentration of the electroactive species of the electrode (Γ) can be calculated from the cyclic voltammograms by the Eq. (5) (Li et al., 2014a, 2014b)

$$\Gamma = Q/nFA \tag{5}$$

The calculated Γ value is 2.05×10^{-8} mol/cm^2, it is four orders of magnitude higher than that (2.86×10^{-12} mol/cm^2) at the bare GCE, indicating a saturated adsorption of the glucose at the surface of Cu_2O–CLGNs /GCE electrode.

Electrochemical impedance spectroscopy (EIS) was used to investigate the interface properties of different modified electrode. Fig. 4 represents the Nyquist diagrams of the Au/GCE, Cu_2O–CLGNs/GCE electrode and Cu_2O/GCE electrodes in the presence of 5 mM $K_3[Fe(CN)_6]$ with 0.1 M KCl as the supporting electrolyte, which show a semicircle portion and a linear portion. The semicircle portion at higher frequencies is due to the electron transfer limited process, and the linear portion at lower frequencies results from the diffusion process (Kang et al., 2009). The electron transfer resistance (R_{ct}) at the electrode surface can be quantified using the semicircle diameter of the Nyquist plots. As one can see from the Fig. 4, the diameter of Nyquist circle on Au/GCE electrode was extremely small, indicating that the charge transfer at Au/GCE electrode is quite facile. While for the Cu_2O/GCE electrode, a substantial increase in the diameter of the semicircle was observed, suggesting that the Cu_2O could act as the inert electron and transfer blocking layer, and hinder the electron transfer from the electrolyte to the electrode surface. After anchoring the Cu_2O grains on the surface of CLGNs, the R_{ct} value drastically decreased from 2620 Ω to 1200 Ω, indicating Cu_2O–CLGNs nanocomposite could act as an electron-transfer interface compared to the pure Cu_2O powder, further confirming that the Cu_2O was successfully immobilized on the surface of CLGNs.

3.3. Glucose detection on the Cu_2O–CLGNs/GCE electrode

Fig. S2 shows the differential pulse voltammograms (DPV) results of the Cu_2O–CLGNs/GCE electrode in the presence of various concentrations of glucose in the range of 0–2 mM, with the potential ranging from 0 to 0.75 mV vs. Ag/AgCl in a 100 mM KOH solution. As one can see that the increment of oxidation peaks became larger with the increase of glucose concentration and the oxidation process started at ca. 0.3 V with a peak at about +0.63 V. There is a linear relationship between the peak currents and the concentrations of glucose ranging from 0 to 2 mM (anodic peak currents, $R^2=0.9915$), as shown in the inset chart of Fig. S2, which is primarily due to the special heterodimer junction effect

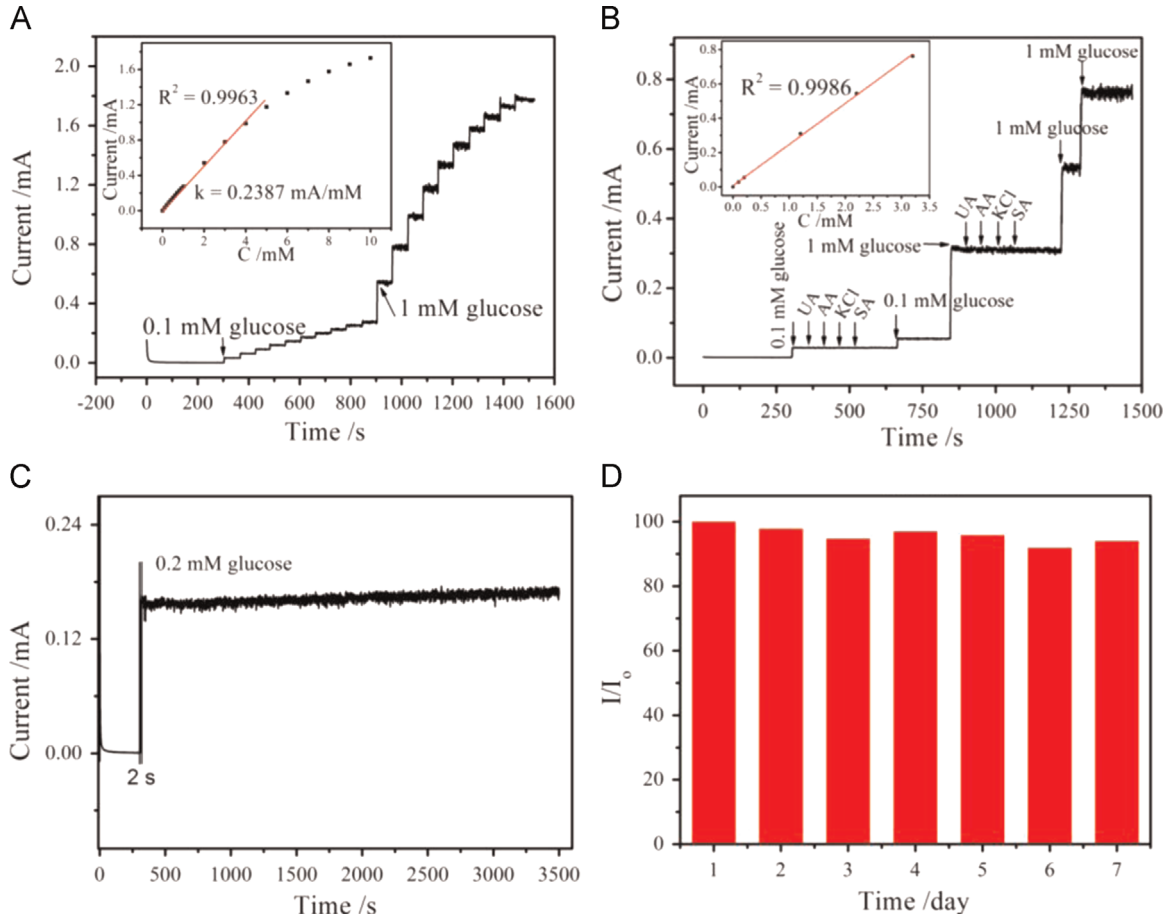

Fig. 5. (A) Amperometric response of the Cu_2O–CLGNs/GCE electrode with successive addition of glucose to the 100 mM KOH solution at regular intervals. The applied potential was +0.63 V vs. Ag/AgCl. (B) Amperometric response to the stepwise injection of UA, AA, KCl and SA, followed by the successive addition of glucose. (C) Amperometric response of the Cu_2O–CLGNs/GCE electrode over a long period of running time. (D) Long-term stability of the Cu_2O–CLGNs-modified electrode.

between Au and Cu_2O, leading to the feasibility of a high conduction pathway of electrons from the analyte and the electrode.

Fig. 5A shows the amperometric responses at the applied potential of 0.63 V of Cu_2O–CLGNs/GCE electrode with successive increments of the glucose concentration from 0 to 10 mM. The Cu_2O–CLGNs/GCE electrode responds rapidly to the changes in glucose concentration and displays a linear shape over a range of concentrations between 0.1 mM and 5 mM (inset of Fig. 5A), and the current response equation is I (mA)=0.2387C+0.027 (mM), with a correlation coefficient of 0.9963. The sensitivity estimated from the linear region of the calibration curve was 1215.7 μA mM^{-1} cm^{-2}, and the detection limit was calculated to be 1.83 μM, which is much lower than the normal blood glucose level of 4.4–6.6 mM (Zhang et al., 2014b).

Some species, such as uric acid (UA), ascorbic acid (AA), potassium chloride (KCl) and sodium ascorbate (SA), were usually coexisting with glucose and possibly interfering biomolecules. We further examined the electrochemical responses (Fig. 5B) of Cu_2O–CLGNs/GCE electrode in the process that UA, AA, KCl and SA with a concentration of 2 μM, were adding into glucose test system at the potential of +0.63 V. The responses of the interfering species are insignificant and the Cu_2O–CLGNs/GCE electrode still have a good linear relation (R^2=0.998). The observations suggest that the Cu_2O–CLGNs hybrid nanostructures demonstrate good specificity for glucose detection in the presence of relatively low concentrations of co-existing interfering agents and adapt to the complicated test system.

Furthermore, the stability and repeatability of the Cu_2O–CLGNs/GCE electrode were investigated by measuring the amperometric response over a long period. Fig. 5C shows the response of the Cu_2O–CLGNs/GCE electrode to 0.2 mM glucose in 100 mM KOH solution at +0.63 V over a long period of running time. As one can see that, the current response presents a finite increase about 6% over a period of more than 50 min, suggesting the high stability of the proposed electrode. This result also implied that the surface properties (such as surface area and electrochemical activity) of Cu_2O–CLGNs compound had not obvious change under the continuous measurement of glucose (Han et al., 2014). In addition, the Cu_2O–CLGNs glucose sensors also exhibit a fast response time in less than 2 s as labeled in Fig. 5D. Seven successive measurements were performed to test storage stability of the Cu_2O–CLGNs/GCE electrode in seven days (1 measurement per day, the electrode was stored at the room temperature). The voltammetric response was no clear decrease and still retained 94.01% value of the initial response, indicating that the Cu_2O–CLGNs/GCE sensor is stable and suitable for the repeated detection of glucose. Table S1 represents a comparison of the sensitivity, linear range, detection limit and response time of analytical parameters of some reported glucose biosensors. It is obviously shown that the Cu_2O–CLGNs sensor exhibits better performances than some of the reported enzymatic and nonenzymatic glucose sensors in terms of high sensitivity and short response time.

3.4. Determination of glucose in human serum samples

In order to evaluate the feasibility of the Cu_2O–CLGNs/GCE electrode, it was used to detect the glucose concentrations in human serum. Briefly, 200 μL serum samples were added into

Table 1
Glucose determination in human blood serum samples (mean ± SD, $n=3$).

Sample no.	Concentrations of glucose (mM)		Deviation rate (%)
	Determination by Cu_2O–CLGNs/GCE bioelectrode (mM)	Determination by automatic biochemical analyzer (mM)	
1	8.8 ± 0.47	9.2	5.3
2	6.8 ± 0.34	7.1	5.0
3	6.6 ± 0.39	6.7	5.9
4	4.4 ± 0.098	4.2	2.2

20 mL KOH (100 mM) solution, and then the current response was recorded by chronoamperometry. By substituting the value into the calibration curve, the concentration of glucose in the human serum sample was calculated. As shown in Table 1, the fund values of glucose by the proposed method are compared with those obtained by an automatic biochemical analyzer. The result exhibited that Cu_2O–CLGNs/GCE electrode was practical and effective for the determination of glucose in actual human serum samples.

4. Conclusions

The Cu_2O nanograins can be well anchored on the surface of highly roughened spiky Au nanotubes through a seeding growth synthesis. The composition of the active Cu_2O with conductive noble metal nanostructures is proposed as a promising method to combine both of their advantages for constructing the glucose biosensors. Thus the performance of the resulting electrode was improved greatly compared with that of GCE electrode modified by Cu_2O nanograins or CLGNs alone by virtue of the synergy effect. The electrochemical measurements indicated that Cu_2O–CLGNs/GCE electrode displayed a wide linear range from 0.1 to 5 mM along with the good stability, high sensitivity 1215.7 $\mu A\ mM^{-1}\ cm^{-2}$ and faster response time (less than 2 s) because of the large surface area and fast electron transfer between metal oxide and metals. In addition, the interference from uric acid, ascorbic acid, potassium chloride and sodium ascorbate that usually coexist with glucose in real samples was negligible. The determination of glucose in human serum samples showed that the Cu_2O–CLGNs/GCE electrode was practical and effective for testing glucose in actual human serum samples. Therefore the Cu_2O–CLGNs hybrid nanostructures provide a promising model for developing the novel nonenzymatic glucose biosensors.

Acknowledgments

We thank Dr. Chuansheng Ma from the International Center for Dielectric Research, Xi'an Jiaotong University, for their support with TEM and SEM. This work is supported by National Natural Science Foundation of China (No. 51271135), the Program for New Century Excellent Talents in University (No. NCET-12-0455), the Fundamental Research Funds for the Central Universities, and the Natural Science Foundation of Shanxi Province and the project of Innovative Team of Shanxi Province (Nos. 2015JM5166 and 2013KCT-05).

Appendix A. Supplementary information

Supplementary data associated with this article can be found in the online version at http://dx.doi.org/10.1016/j.bios.2015.07.074.

References

Ahmad, R., Vaseem, M., Tripathy, N., Hahn, Y.-B., 2013. Anal. Chem. 85 (21), 10448–10454.
Ahmadalinezhad, A., Chatterjee, S., Chen, A., 2013. Electrochim. Acta 112, 927–932.
Bi, Y., Hu, H., Lu, G., 2010. Chem. Commun. 46 (4), 598–600.
Cao, X., Wang, N., Jia, S., Shao, Y., 2013. Anal. Chem. 85 (10), 5040–5046.
Chang, Y., Zeng, H.C., 2004. Cryst. Growth Des. 4 (2), 273–278.
Chen, A., Chatterjee, S., 2013. Chem. Soc. Rev. 42 (12), 5425–5438.
Cherevko, S., Chung, C.-H., 2010. Talanta 80 (3), 1371–1377.
Ci, S., Huang, T., Wen, Z., Cui, S., Mao, S., Steeber, D.A., Chen, J., 2014. Biosens. Bioelectron. 54, 251–257.
Ding, Y., Wang, Y., Su, L., Bellagamba, M., Zhang, H., Lei, Y., 2010a. Biosens. Bioelectron. 26 (2), 542–548.
Ding, Y., Wang, Y., Su, L., Zhang, H., Lei, Y., 2010b. J. Mater. Chem. 20 (44), 9918–9926.
Ding, Y., Liu, Y., Parisi, J., Zhang, L., Lei, Y., 2011. Biosens. Bioelectron. 28 (1), 393–398.
Duan, H., Xu, D., Li, W., Xu, H., 2008. Catal. Lett. 124 (3–4), 318–323.
Elahi, M.Y., Khodadadi, A.A., Mortazavi, Y., 2014. J. Electrochem. Soc. 161 (5), B81–B87.
Feng, X., Guo, C., Mao, L., Ning, J., Hu, Y., 2014. J. Am. Ceram. Soc. 97 (3), 811–815.
Guo, M.-m, Wang, P.-s, Zhou, C.-h, Xia, Y., Huang, W., Li, Z., 2014. Sens. Actuators B 203, 388–395.
Han, L., Zhang, S., Han, L., Yang, D.-P., Hou, C., Liu, A., 2014. Electrochim. Acta. 138, 109–114.
Hong, F., Sun, S., You, H., Yang, S., Fang, J., Guo, S., Yang, Z., Ding, B., Song, X., 2011. Cryst. Growth Des. 11 (9), 3694–3697.
Hsu, C.-W., Wang, G.-J., 2014. Biosens. Bioelectron. 56, 204–209.
Hua, Q., Shi, F., Chen, K., Chang, S., Ma, Y., Jiang, Z., Pan, G., Huang, W., 2011. Nano Res. 4 (10), 948–962.
Huang, Y., Zhang, W., Xiao, H., Li, G., 2005. Biosens. Bioelectron. 21, 817–821.
Huo, H., Guo, C., Li, G., Han, X., Xu, C., 2014. RSC Adv. 4 (39), 20459–20465.
Hwa, K.-Y., Subramani, B., 2014. Biosens. Bioelectron. 62, 127–133.
Kang, X., Wang, J., Wu, H., Aksay, I.A., Liu, J., Lin, Y., 2009. Biosens. Bioelectron. 25 (4), 901–905.
Kuo, C.-H., Huang, M.H., 2010. Nano Today 5 (2), 106–116.
Lang, X.-Y., Fu, H.-Y., Hou, C., Han, G.-F., Yang, P., Liu, Y.-B., Jiang, Q., 2013. Nat. Commun. 4, 1–8.
Li, J., Yang, Z., Tang, Y., Zhang, Y., Hu, X., 2013. Biosens. Bioelectron. 41, 698–703.
Li, J., Yang, J., Zhou, J., Wei, Q., Huang, F., 2014a. RSC Adv. 4, 61831–61840.
Li, M., Bo, X., Zhang, Y., Han, C., Guo, L., 2014b. Biosens. Bioelectron. 56, 223–230.
Liu, M., Liu, R., Chen, W., 2013a. Biosens. Bioelectron. 45, 206–212.
Liu, S., Zhang, C., Yuan, L., Bao, J., Tu, W., Han, M., Dai, Z., 2013b. Part. Part. Syst. Charact. 30 (6), 549–556.
Luo, M.Z., Baldwin, R.P., 1995. J. Electroanal. Chem. 387 (1–2), 87–94.
Meng, F., Shi, W., Sun, Y., Zhu, X., Wu, G., Ruan, C., Liu, X., Ge, D., 2013. Biosens. Bioelectron. 42, 141–147.
Minteer, S.D., Atanassov, P., Luckarift, H.R., Johnson, G.R., 2012. Mater. Today 15 (4), 166–173.
Niu, X., Chen, C., Zhao, H., Chai, Y., Lan, M., 2012. Biosens. Bioelectron. 36 (1), 262–266.
Sun, S., Zhou, F., Wang, L., Song, X., Yang, Z., 2010. Cryst. Growth Des. 10 (2), 541–547.
Sun, S., Zhang, X., Sun, Y., Yang, S., Song, X., Yang, Z., 2013. ACS Appl. Mater. Interfaces 5 (10), 4429–4437.
Torto, N., Ruzgas, T., Gorton, L., 1999. J. Electroanal. Chem. 464 (2), 252–258.
Wang, A.-J., Feng, J.-J., Li, Z.-H., Liao, Q.-C., Wang, Z.-Z., Chen, J.-R., 2012. CrystEngComm 14 (4), 1289–1295.
Wang, J., Thomas, D.F., Chen, A., 2008. Anal. Chem. 80 (4), 997–1004.
Wang, X., Liu, E., Zhang, X., 2014. Electrochim. Acta 130, 253–260.
Wu, H.-X., Cao, W.-M., Li, Y., Liu, G., Wen, Y., Yang, H.-F., Yang, S.-P., 2010. Electrochim. Acta 55 (11), 3734–3740.
Xiao, F., Li, Y., Gao, H., Ge, S., Duan, H., 2013. Biosens. Bioelectron. 41, 417–423.
Xu, C., Sun, F., Gao, H., Wang, J., 2013. Anal. Chim. Acta 780, 20–27.
Xu, F., Cui, K., Sun, Y., Guo, C., Liu, Z., Zhang, Y., Shi, Y., Li, Z., 2010. Talanta 82 (5), 1845–1852.
Yang, A., Bi, J., Yang, S., Zhang, J., Chen, A., Liang, S., 2014a. RSC Adv. 4 (86), 45856–45861.
Yang, L., Zhang, Y., Chu, M., Deng, W., Tan, Y., Ma, M., Su, X., Xie, Q., Yao, S., 2014b. Biosens. Bioelectron. 52, 105–110.
Yang, S., Luo, X., 2014. Nanoscale 6 (9), 4438–4457.
Yang, W., Ratinac, K.R., Ringer, S.P., Thordarson, P., Gooding, J.J., Braet, F., 2010. Angew. Chem. Int. Ed. 49 (12), 2114–2138.
Yu, X., Zhuang, L., Yang, S., Yang, Z., Song, X., Ding, B., 2010. Coll. Surf. A 372 (1–3), 22–27.
Zhang, Q., Zhang, K., Xu, D., Yang, G., Huang, H., Nie, F., Liu, C., Yang, S., 2014a. Prog. Mater. Sci. 60, 208–337.
Zhang, X., Sun, S., Lv, J., Tang, L., Kong, C., Song, X., Yang, Z., 2014b. J. Mater. Chem. A 2 (26), 10073–10080.
Zhang, Y., Li, Y., Wu, W., Jiang, Y., Hu, B., 2014c. Biosens. Bioelectron. 60, 271–276.
Zhou, D.-L., Feng, J.-J., Cai, L.-Y., Fang, Q.-X., Chen, J.-R., Wang, A.-J., 2014. Electrochim. Acta 115, 103–108.
Zhuang, Z., Su, X., Yuan, H., Sun, Q., Xiao, D., Choi, M.M.F., 2008. Analyst 133 (1), 126–132.